

## Article

# Expanded Illite Filler in UV-Curable Polymer Electrolytes for All-Solid-State Li-Ion Batteries

Minseong Bae <sup>1,†</sup>, Seongki Ahn <sup>2,†</sup> , Sunkyung You <sup>1</sup>, Jae-kwang Kim <sup>1</sup> , Daewon Kim <sup>3</sup>, Hanjoo Kim <sup>3</sup>, Hong-Il Kim <sup>1,\*</sup> and Jinjoo Park <sup>1,\*</sup>

<sup>1</sup> Department of Energy Convergence Engineering, Cheongju University, Cheongju 28503, Republic of Korea; hheli48@daum.net (M.B.); skyou@cju.ac.kr (S.Y.); jaekwang@cju.ac.kr (J.-k.K.)

<sup>2</sup> School of Food Biotechnology and Chemical Engineering, Research Center of Chemical Technology, Hankyong National University, Anseong 17579, Republic of Korea; skahn@hknu.ac.kr

<sup>3</sup> Pureechem, Namseok-ro, Nami-myeon, Seowon-gu 151-35, Cheongju 28182, Republic of Korea; dwkim@pureechem.com (D.K.); hjkim@pureechem.com (H.K.)

\* Correspondence: hikim007@cju.ac.kr (H.-I.K.); jwjh3516@cju.ac.kr (J.P.)

† These authors contributed equally to this work.

**Abstract:** In this study, we explored the potential of illite sourced from Yeongdong-eup, South Korea, as a filler in polymer electrolytes for all-solid-state Li-ion batteries. The illite was expanded (EI) by acid treatment and UV curing was employed to synthesize the polymer electrolytes. The Li<sup>+</sup> ionic conductivity of the polymer electrolytes was measured at various EI contents, revealing the highest conductivity of  $1.08 \times 10^{-2} \text{ S cm}^{-1}$  at 4 wt% of the EI. The electrochemical performance of NMC cells assembled with the EI-incorporated polymer electrolyte showed a good discharge capacity of over 158.6 mAh g<sup>-1</sup> with a coulombic efficiency of 99%. These findings demonstrate the significant potential of EI as a sustainable and efficient filler material for enhancing the performance of polymer-based all-solid-state Li batteries. This study highlighted the applicability of illite sourced from South Korea and its potential contribution to the development of polymer-based all-solid-state batteries.

**Keywords:** illite; polymer electrolyte; solid-state batteries; lithium-ion batteries



**Citation:** Bae, M.; Ahn, S.; You, S.; Kim, J.-k.; Kim, D.; Kim, H.; Kim, H.-I.; Park, J. Expanded Illite Filler in UV-Curable Polymer Electrolytes for All-Solid-State Li-Ion Batteries. *Coatings* **2024**, *14*, 1158. <https://doi.org/10.3390/coatings14091158>

Academic Editor: Gianfranco Carotenuto

Received: 2 August 2024

Revised: 20 August 2024

Accepted: 5 September 2024

Published: 9 September 2024



**Copyright:** © 2024 by the authors. Licensee MDPI, Basel, Switzerland. This article is an open access article distributed under the terms and conditions of the Creative Commons Attribution (CC BY) license (<https://creativecommons.org/licenses/by/4.0/>).

## 1. Introduction

Lithium-ion batteries (LIBs) have been widely used in various fields, including small electronic devices, wearable devices, energy storage systems, and large-scale applications, such as electric vehicles (EVs) and energy storage systems (ESS), owing to their advantages, such as no memory effect, high operating voltage, and stable cyclability [1–6]. Despite these advantages, recent safety issues of LIBs, such as thermal runaway, have received significant attention annually, prompting extensive research to address their safety concerns [7–11].

To solve the safety issues of LIBs, numerous studies have focused on the development of flame-retardant materials and the synthesis and application of nonflammable solid-state electrolytes [12–15], and aqueous electrolytes [16–19]. Among these solutions, one promising approach is the development of solid-state electrolytes [20–22].

Solid electrolytes are a research area of significant interest because they allow the construction of more cells within the same volume and offer higher stability than conventional flammable organic liquid electrolytes. Therefore, active research has focused on developing solid-state electrolytes to replace organic electrolytes in LIBs [23–25].

Solid-state electrolytes can be categorized into three classes: oxide-based [26–28], sulfide-based [29–31], and polymer-based [32–37]. Among these, polymer-based solid-state electrolytes stand out because of their good flexibility, high Li-ion conductivity, and relatively simple manufacturing process compared with oxide- and sulfide-based electrolytes. However, polymer-based solid-state electrolytes (PBSSEs) present significant challenges because of their poor mechanical properties. To address this issue, various fillers, such as

carbon black, non-carbon materials, and clay minerals, have been explored to enhance their mechanical strength.

Illite, a clay mineral, is widely used as a filler in polymer materials because of its advantages, such as its low cost, abundance in nature, and non-toxicity [38–42]. These properties render illite a promising candidate for improving the mechanical properties of polymer-based solid-state electrolytes. Thus, illite has emerged as an attractive filler.

To the best of our knowledge, we are the first to report the synthesis of a PBSSE using an expanded illite (EI) filler, which was sourced and produced in Yeongdong-eup, Republic of Korea, for all-solid-state Li-ion batteries (ASSLIBs). Furthermore, we have revealed the electrochemical advantages of EI as a clay-type filler for PBSSEs. To effectively utilize the illite, we increased the interlayer distance of pure illite to obtain EI. We found that the PBSSE synthesized with 4 wt% of the EI had the highest Li<sup>+</sup> ionic conductivity of  $2.9 \times 10^{-3} \text{ S cm}^{-1}$ . This is because the EI filler reduced the crystallinity of the polymer matrix and accelerated the Li<sup>+</sup> ion mobility. The ASSLIB assembled with an NCM cathode and a Li-metal anode showed a favorable discharge capacity of 153 mAh g<sup>-1</sup> with a coulombic efficiency of 99%.

## 2. Materials and Methods

### 2.1. Preparation of the EI

Pure illite (Yongkoong Illite Co., Ltd., Yongkoong, Republic of Korea) was used to prepare the EI. Pure illite was ball milled with zirconia balls for 12 h to remove impurities. After ball milling, the pure illite solution was dried at 80 °C for 12 h. Thereafter, the dried illite was calcinated at 600 °C for 1 h. The heated illite was mixed with 2M HNO<sub>3</sub> (Sigma Aldrich, Saint Louis, MO, USA) at 95 °C for 3 h and washed with deionized water until its pH was 7. The acid-treated illite was magnetically stirred with dimethyl sulfoxide (DMSO, Tokyo Chemical Industry Co., Ltd., Tokyo, Japan) and deionized water for 1 h. Subsequently, the mixture was placed in a microwave for 1 h for the interaction of the DMSO with the interlayer of the illite. Thereafter, the sample was sonicated at 70 °C for 1 h and centrifuged at 4000 rpm.

### 2.2. Synthesis of the PBSSE

The PBSSE was synthesized using a monomer mixture and an electrolyte mixture. To prepare the monomer mixture, 95 wt% of ethoxylated trimethylolpropane triacrylate (Sigma-Aldrich, USA) as a monomer and 5 wt% of 2-Hydroxy-2-methylpropiophenone (Tokyo Chemical Industry Co., Ltd., Tokyo, Japan) as a photoinitiator were mixed by a magnetic stirrer for 30 min. Then, 1M lithium bis(trifluoromethylsulfonyl)imide (Sigma-Aldrich, USA) in trimethylolpropane ethoxylate triacrylate (Sigma-Aldrich, USA) as an ionic liquid were mixed as an electrolyte mixture. Afterward, 50 wt% of the monomer mixture and 50 wt% of the electrolyte mixture were mixed for 5 hrs. To synthesize the PBSSE, the above mixture was mixed with the EI (0–8 wt%) and then casted onto a glass plate and exposed to UV irradiation (365 nm) for 55 sec.

### 2.3. Materials and Electrochemical Characterization

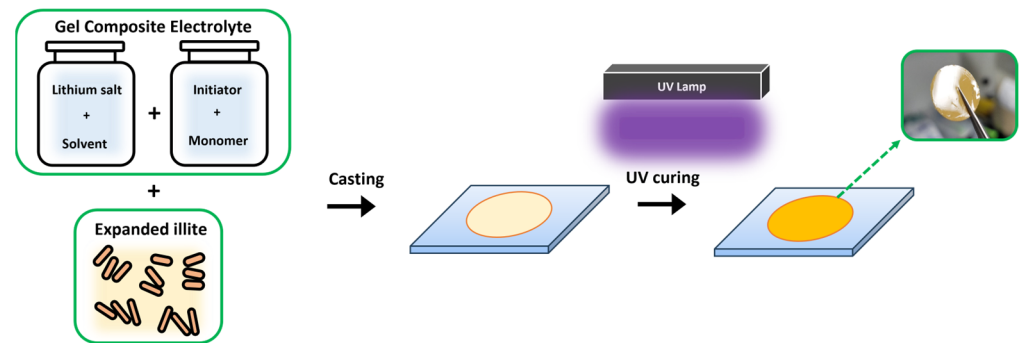
The morphologies of the pure illite, EI, and PBSSE were examined using field-emission scanning electron microscopy (FE-SEM; MIRA 3, Tescan, Kohoutovice, Czech Republic). The particle distributions of the samples were investigated using a particle size analyzer (PSA, LA-960, Horiba, Kyoto, Japan). The crystallinity of all samples was measured using X-ray diffraction (XRD, SDT-Q 600, TA instruments, New Castle, DE, USA). Fourier transform infrared spectroscopy (FT-IR, Frontier, PerkinElmer, Singapore) was performed using the PBSSE, depending on the presence or absence of the EI. Thermogravimetric analysis (TGA, SDT-Q 600, TA instruments, USA) was conducted at temperatures up to 500 °C. The ionic conductivity of the PBSSE was analyzed by electrochemical impedance spectroscopy (EIS, ZIVE SP2, Wonatech, Seoul, Republic of Korea) in the frequency range of 1–2 MHz with an amplitude of 100 mV, and was calculated using Equation (1).

$$\sigma = l / (R * A) \quad (1)$$

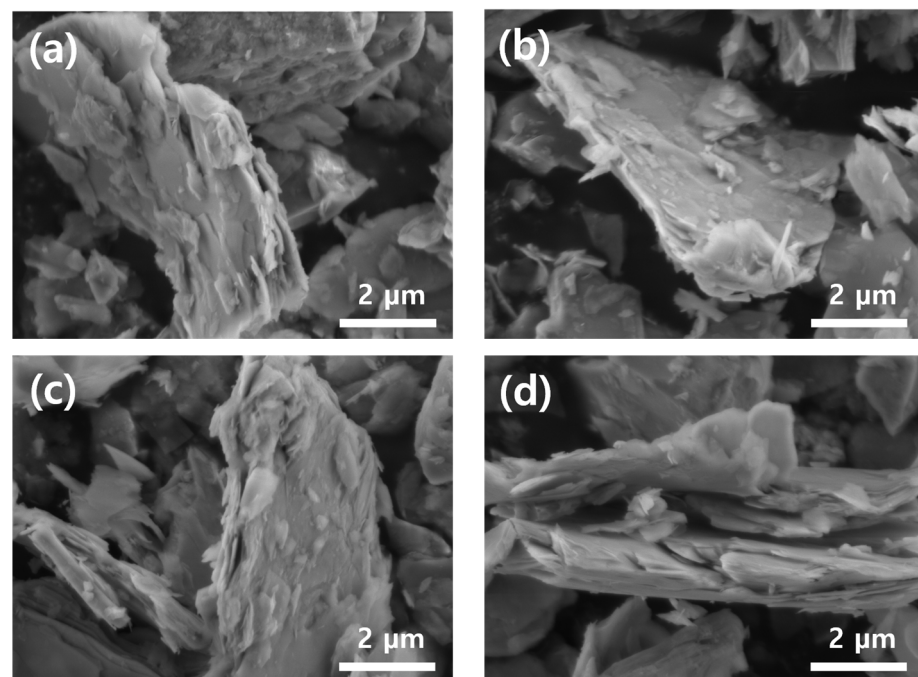
Here,  $\sigma$  represents an ionic conductivity ( $S \text{ cm}^{-1}$ ),  $l$  represents the thickness of the PBSSE (cm),  $R$  represents the resistance measured by EIS (ohm), and  $A$  represents the area of the PBSSE ( $\text{cm}^{-2}$ ). The electrochemical properties of the ASSLIB assembled with the NCM cathode, PBSSE, and Li-metal anode were tested with a voltage range from 3.0 to 4.2 V at a 0.2 C-rate.

### 3. Results and Discussion

Figure 1 shows the synthesis of the PBSSE and a photograph of the PBSSE after UV curing. As shown in Figure 1, the PBSSE is flexible and yellow. It is expected that the PBSSE synthesized using an EI filler will have improved mechanical properties. In addition, we found that the EI was well dispersed in the PBSSE, giving it a uniform yellow color. The EI is obtained through a complex process involving heat, acid, and microwave treatments. To confirm the process that affected the expansion of pure illite, changes in the morphology of the illite depending on each process were measured using FE-SEM analysis, as shown in Figure 2.

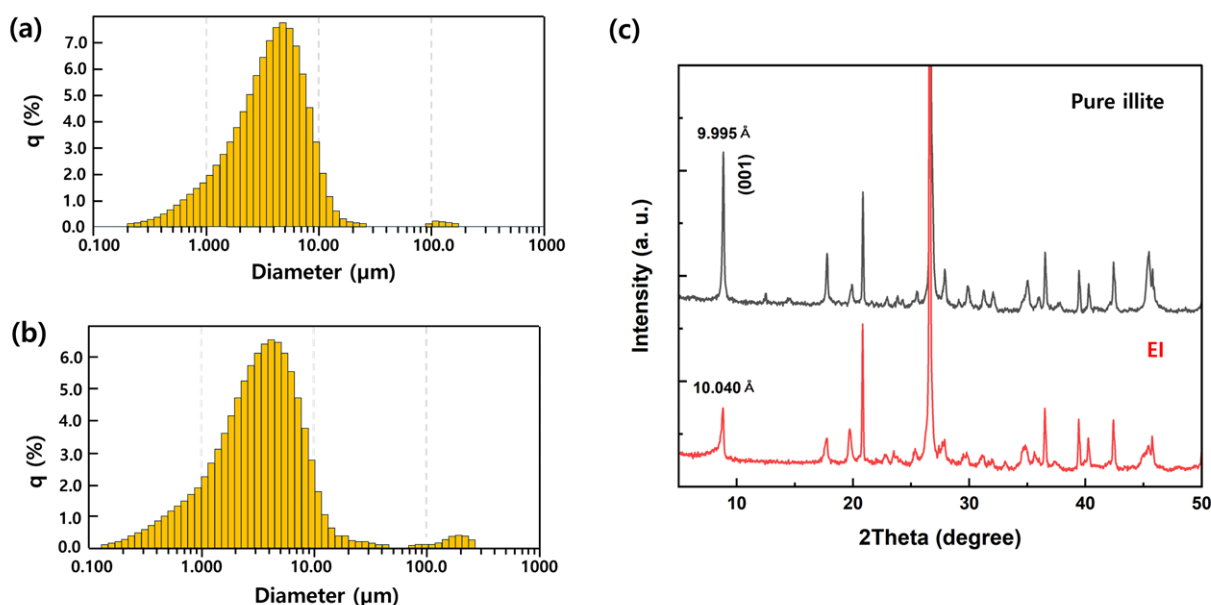


**Figure 1.** Synthesis process of the polymer-based solid-state electrolytes by photopolymerization using expanded illite.



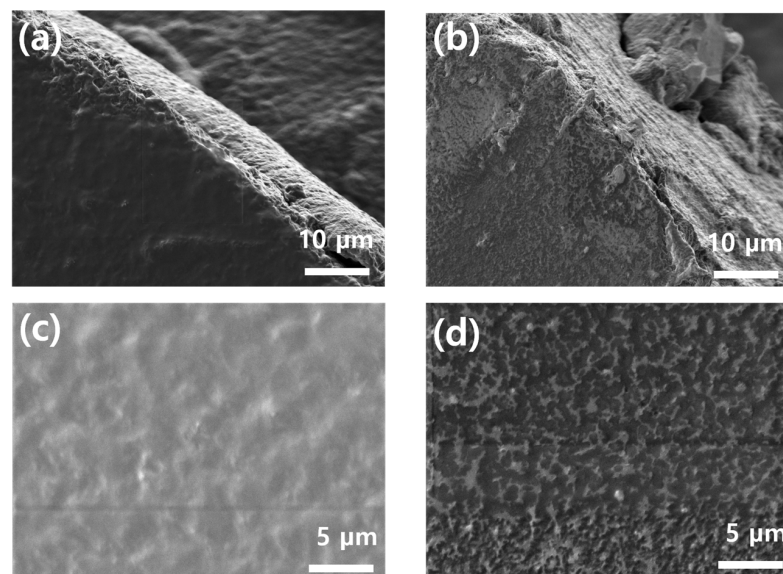
**Figure 2.** Field emission scanning electron microscope images of the (a) pure illite, (b) heat-treated illite, (c) heat- and acid-treated illite, and (d) heat-, acid-, and microwave-treated illite.

Figure 2a–c shows the morphologies of the pure illite, heat-treated illite, and heat- and acid-treated illite. As shown in this figure, we did not find a layered structure in the illite. In contrast, in Figure 2d, the heat-, acid-, and microwave-treated illite shows an expanded layer structure throughout the illite. This is because DMSO was intercalated into the illite interlayer, and the microwave treatment affected the DMSO, resulting in the expansion of the illite structure [43]. We believed that the expansion of the illite induced by the DMSO and the complex procedures performed above would affect the size of the entire particle. To verify this assumption, PSA was conducted. Figure 3 shows the PSA results for the pure illite and EI. The pure illite has a mean particle size of 5.28  $\mu\text{m}$ , while the EI has a larger mean size of 8.26  $\mu\text{m}$ . Table S1 shows detailed information on the PSA analysis. These results reveal that the expansion of illite not only expands the interlayer in the illite but also enlarges the illite particle size. To compare the crystallinity of the pure illite and EI, an XRD study was conducted with Cu K $\alpha$  radiation at 40 kV and 15 mA. Figure 3c shows the XRD patterns of both samples. The peak located at approximately  $9^\circ$  is assigned to the basal d(001) diffraction peak of illite. In the XRD pattern of pure illite, we confirmed that the pure illite has a basal d(001) diffraction peak at  $d = 9.995 \text{ \AA}$ . However, the EI shows a new d(001) diffraction peak at  $d = 10.040 \text{ \AA}$ . Complex processes, including heating, acidification, and microwave treatment using DMSO, can increase the interlayer distance [44]. Thus, we believe that the illite expansion process was successfully conducted.



**Figure 3.** Particle size analysis results of the (a) pure illite and (b) expanded illite. (c) X-ray diffraction patterns of the purified illite and expanded illite obtained by heat, acid, and microwave treatment using dimethyl sulfoxide.

We fabricated the PBSSE with and without the EI by photopolymerization. As shown in Figure S1, the colors of the PBSSE are different. The PBSSE prepared without the EI was white, whereas the PBSSE with the EI was yellow. Figure 4 shows the morphology of the PBSSE depending on the presence or absence of the EI. Figure 4a,b shows side views of the PBSSE with and without the EI. As shown in these images, we confirmed that the PBSSE without the EI had smoother characteristics. In contrast, the PBSSE fabricated with the EI appeared to have a rougher surface. In the top views of both samples in Figure 4c,d, the PBSSE with the EI has a rough surface. From these results, we revealed that the illite filler affects the surface characteristics not only on the top surface but also on the sides. The rough surface of the PBSSE using the EI can lead to a larger contact area between the cathode and anode, resulting in the enhancement of the electrochemical reaction.



**Figure 4.** Field emission scanning electron microscope images of the polymer-based solid-state electrolytes. (a) Side image of the polymer-based solid-state electrolytes without expanded illite, and (b) with expanded illite. Top-view of the polymer-based solid-state electrolytes (c) without expanded illite, and (d) with expanded illite.

To investigate the dependence of the crystallinity of the PBSSE on the use of the EI filler, XRD analysis was conducted on both samples. Figure 5 shows the XRD patterns of the PBSSE with and without the EI filler. There are three peaks located at  $8.9^\circ$ ,  $17.7^\circ$ , and  $26.7^\circ$ , corresponding to the crystalline plane of (001), (004), and (006) of the EI, respectively. As shown in the XRD patterns, the PBSSE and PBSSE with the EI had similar peaks located at  $31^\circ$ , which were attributed to the polymer matrix. A new peak located at  $27^\circ$ , which is a feature of the EI, is observed, as shown in the XRD pattern of the EI (blue line) in Figure 5. Additionally, all peaks of the PBSSE with the EI were shifted from those of the original PBSSE because the polymer matrix might influence the crystallinity of the PBSSE with the EI. From the XRD results, we confirmed that the use of the EI filler decreased the crystallinity of the PBSSE.

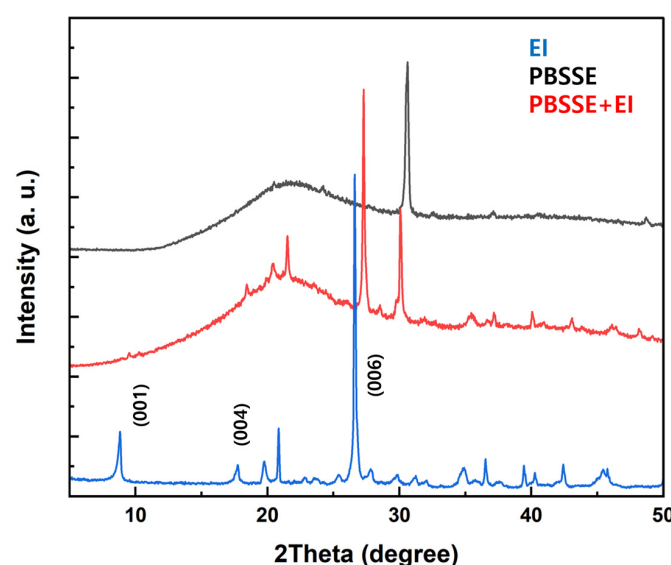


**Figure 5.** X-ray diffraction patterns of the expanded illite powder, polymer-based solid-state electrolytes synthesized without any filler, and polymer-based solid-state electrolytes fabricated with the expanded illite filler.

We investigated the impact of the EI filler on the PBSSE through morphological and crystallographic analyses. Based on these results, we believe that the EI filler can affect the morphology and crystallinity of the PBSSE. However, the use of the EI filler does not adversely affect the stability of the polymer structure. To consider this aspect, we performed FT-IR analysis of the PBSSE and PBSSE with the EI. Figure 6 shows the FT-IR spectra of the photopolymerized PBSSE without and with the EI in the range of 1500–3200  $\text{cm}^{-1}$ . The peak located around 1653  $\text{cm}^{-1}$  is assigned to the acrylic C=C bond. The ester carbonyl -CO- bond was observed at 1735  $\text{cm}^{-1}$  in both samples. In addition, we checked the stretching vibrations of the methyl (-CH<sub>3</sub>) and methylene (-CH<sub>2</sub>) groups [45]. Through FT-IR investigations, we confirmed that the EI filler did not affect the chemical bonding of the polymer matrix, indicating that the polymer matrix of the PBSSE without or with the EI filler is similar.

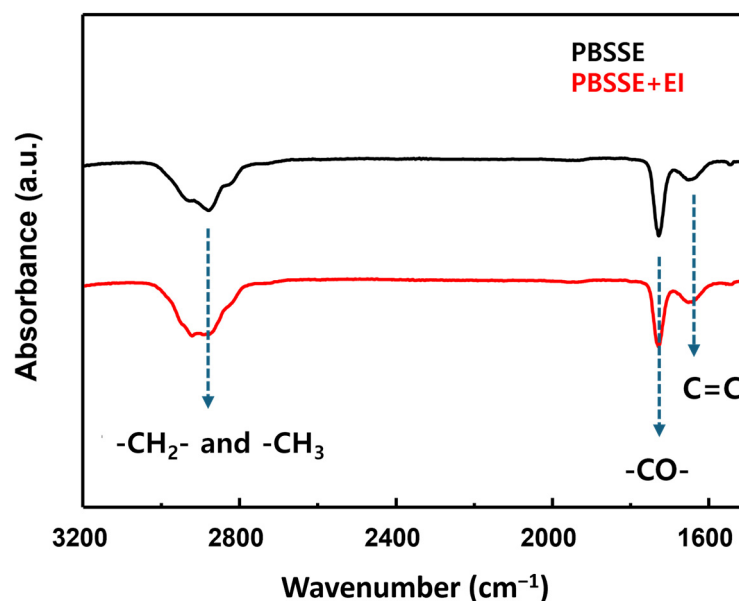


**Figure 6.** Fourier transform infrared spectra of the polymer-based solid-state electrolytes without and with the expanded illite filler synthesized by photopolymerization.

To determine the optimal PBSSE conditions for Li<sup>+</sup> ionic conductivity, we tested the ionic conductivity of the PBSSE with varying amounts of the EI, ranging from 0 to 8 wt%. The ionic conductivity was measured by electrochemical impedance spectroscopy using a symmetric cell assembled with two stainless-steel electrodes. At room temperature, the PBSSE fabricated without the EI filler has an ionic conductivity of  $2.05 \times 10^{-3} \text{ S cm}^{-1}$ . Generally, in solid-state electrolytes, those with ionic conductivity over  $10^{-4} \text{ S cm}^{-1}$  have a favorable value of ionic conductivity because liquid-phase electrolytes have an ionic conductivity of around  $>10^{-3} \text{ S cm}^{-1}$ . As the amount of the EI filler increased up to 4 wt%, the ionic conductivity also increased to  $3.02 \times 10^{-3} \text{ S cm}^{-1}$ . However, the ionic conductivity decreased when more than 6 wt% of the EI filler was added. This is because a large amount of the EI filler significantly increases the viscosity of the solution used to fabricate the PBSSE, which negatively affects its formability. We compared the ionic conductivity of the PBSSE without and with 4 wt% of the EI filler at different temperatures from 40 to 50 °C. As shown in Figure 7b, the PBSSE synthesized by photopolymerization without the EI filler has ionic conductivities of 9.61, 7.72, 5.90, 4.71, and  $3.40 \times 10^{-3} \text{ S cm}^{-1}$  at 50, 46, 44, 42, and 40 °C, respectively. The PBSSE prepared with the EI filler shows improved ionic conductivities of  $1.08 \times 10^{-2}$ , 9.44, 7.85, 6.49, and  $4.01 \times 10^{-3} \text{ S cm}^{-1}$  at the same temperatures. This improvement occurred because the EI filler decreased the crystallinity of the polymer matrix, resulting in an enhanced ionic conductivity. Table 1 presents detailed information on the ionic conductivities of both samples.

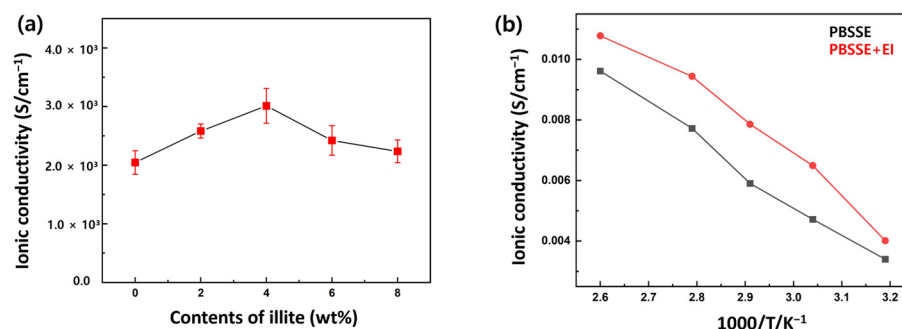


**Figure 7.** (a) Ionic conductivity of the polymer-based solid-state electrolytes depending on the amounts of expanded illite filler from 0 to 8 wt% and (b) comparison of the ionic conductivity of the polymer-based solid-state electrolytes without or with the expanded illite filler at different temperatures.

**Table 1.** Ionic conductivity (S cm<sup>-1</sup>).

	Ionic Conductivity (S cm <sup>-1</sup> )	
	PBSSE without EI	PBSSE with 4 wt% of EI
2.60	$9.61 \times 10^{-3}$	$1.08 \times 10^{-2}$
2.79	$7.72 \times 10^{-3}$	$9.44 \times 10^{-3}$
2.91	$5.90 \times 10^{-3}$	$7.85 \times 10^{-3}$
3.04	$4.71 \times 10^{-3}$	$6.49 \times 10^{-3}$
3.19	$3.40 \times 10^{-3}$	$4.01 \times 10^{-3}$

Figure S2 shows the TGA graphs of the EI filler, the PBSSE without the EI filler, and the PBSSE prepared with 4 wt% of the EI filler. At 500 °C, the EI filler retained 97.38% of its weight. We assume that the moisture evaporated around 100 °C, indicating that the EI filler contains a small amount of moisture, at approximately 2–3 wt%. The PBSSE and PBSSE with the EI filler had weights of 7.28% and 9.71%, respectively. Although we added 4 wt% of the EI filler to the PBSSE, the weight difference between the two samples was only 2.43 wt%. As aforementioned, the EI filler contained 2–3 wt% moisture. Therefore, the weight difference between the PBSSE without the EI filler and the PBSSE with 4 wt% of the EI filler was less than 4 wt%. Figure S3 illustrates the cell configuration of the ASSLIB. To improve the interface between the cathode and PBSSE, we coated the NMC622 cathode directly, followed by photopolymerization using a UV lamp. In addition, a small amount of liquid electrolyte was added between the PBSSE and Li-metal anode to reduce the interface resistance between the PBSSE and Li anode. The cyclic voltammogram of the ASSLIB assembled with 4% of the EI was tested at different scan rates from 0.1 to 0.5 mV s<sup>-1</sup> (Figure S4). There were two intercalated and de-intercalated peaks observed at approximately 3.4 and 3.9 V. The reason for observing two broad peaks instead of the typical four sharp peaks of the NMC cathode is due to the high interfacial resistance. This result indicates the need to improve the interfacial resistance between the electrode and the PBSSE.

Figure 8a shows the Nyquist plot of the ASSLIB before and after charge/discharge cycling. Before charging, the ASSLIB has a charge transfer resistance ( $R_{ct}$ ) of 483 Ω. We checked that the  $R_{ct}$  value decreased from 483 to 376 Ω after charge/discharge cycling, implying that the electrochemical performance could be improved by the activation process. The galvanostatic charge and discharge test was conducted at a 0.2 C-rate with a voltage range from 3.0 to 4.2 V. Figure 8b shows the charge and discharge curves of the ASSLIB assembled using the NMCC622 cathode, PBSSE (4 wt% of the EI), and Li-metal anode. We confirmed the typical charge and discharge behaviors of the NMC-based cathode. The discharge capacity of the ASSLIB is 151.2, 154.6, 152.7, 150.7, 148.3, and 158.6 mAh g<sup>-1</sup> in the 1st, 5th, 10th, 20th, 30th, and 40th cycle, respectively. This value is similar to that of

typical NMC622 Li-ion batteries assembled using liquid electrolytes. We checked the noise in the charge and discharge curves in the 1st cycle. We assumed that the noise observed in the charge/discharge curve during the 1st cycle was due to the unstable movement of lithium ions within the PBSSE. Because no noise was observed in the subsequent curves, we inferred that normal charge/discharge behavior occurred after the initial activation process. This indicates that an initial activation process is essential for the stable electrochemical behavior of the ASSLIB-comprised PBSSE prepared using an EI filler. Figure 8c shows the cyclability of the ASSLIB assembled with the NMC622 cathode, PBSSE with 4 wt% of the EI filler, and Li-metal anode for 40 cycles at a 0.2 C-rate. The initial discharge capacity was  $150.0 \text{ mAh g}^{-1}$ . The discharge capacity decreased slightly around the 25th cycle, then it increased to  $158.6 \text{ mAh g}^{-1}$  in the 40th cycle. Although unstable electrochemical behavior was observed in the ASSLIBs assembled with the PBSSE (4 wt% of the EI), it was confirmed that the ASSLIB maintained a favorable discharge capacity of over  $150 \text{ mAh g}^{-1}$  during 40 charge/discharge cycles. Figure S5 shows the charge/discharge curves and cyclability of the ASSLIBs with 0% and 8% of the EI. We confirmed that the ASSLIBs assembled with 4% of the EI have the most stable cyclability. This result means that the appropriate amounts of EI affect the electrochemical performances. These results demonstrate the effectiveness of the PBSSE and the EI filler sourced from Yeongdong-eup in the Republic of Korea as solid electrolytes for ASSLIBs.

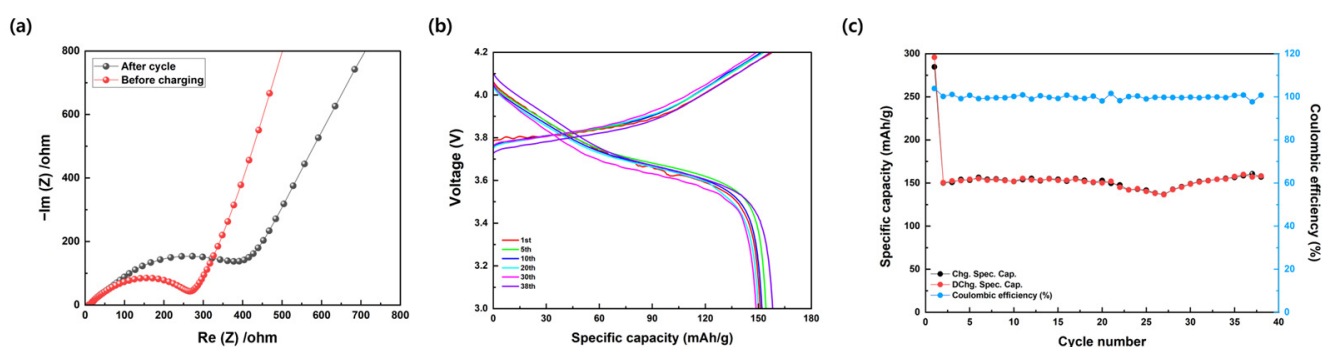


**Figure 8.** Electrochemical performance of the all-solid-state Li-ion batteries assembled with a  $\text{LiNi}_{0.6}\text{Mn}_{0.2}\text{Co}_{0.2}\text{O}_2$  cathode, polymer-based solid-state electrolytes (4 wt% of the expanded illite), and a Li-metal anode: (a) Nyquist plot of the all-solid-state Li-ion batteries before and after cycling, (b) charge and discharge curves at a 0.2 C-rate with a voltage range from 3.0 to 4.2 V, and (c) cyclability of the all-solid-state Li-ion batteries at a 0.2 C-rate for 40 cycles.

#### 4. Conclusions

To the best of our knowledge, this study is the first to use illite mined from Yeongdong-eup, Republic of Korea, as a filler for polymer-based solid electrolytes. We obtained the expanded illite through complex pretreatment processes to utilize the illite more effectively. The PBSSE with 4 wt% of the expanded illite exhibited the highest ionic conductivity of  $1.08 \times 10^{-2} \text{ S cm}^{-1}$ . In the ASSLIBs assembled with an NMC622 cathode and a Li-metal anode, we observed an initial discharge capacity of  $151.2 \text{ mAh g}^{-1}$ , indicating a favorable electrochemical performance. We also discovered that the initial activation process can lead to improved electrochemical reactions in the ASSLIBs. Charge/discharge testing at a 0.2 C-rate demonstrated that the ASSLIB delivered a high discharge capacity of  $158.6 \text{ mAh g}^{-1}$ . This study confirms the effectiveness of illite sourced from Yeongdong-eup, Republic of Korea, and highlights its potential for use in next-generation all-solid-state batteries, which are gaining significant attention in the field of lithium batteries. Furthermore, this research provides a new pathway for enhancing the performance of polymer-based solid electrolytes by utilizing locally sourced, sustainable materials like illite.

**Supplementary Materials:** The following supporting information can be downloaded at: <https://www.mdpi.com/article/10.3390/coatings14091158/s1>, Table S1: Particle size analysis data of the pure

illite and expanded illite; Figure S1: Photo images of the (a) PBSSE without the illite (white color) and (b) PBSSE with 4 wt% of the EI (yellow color); Figure S2: TGA curves of the EI (black line), PBSSE without the EI (blue line), and PBSSE with 4 wt% of the EI (red line); Figure S3: Coin-cell configuration for the ASSLIB. Figure S4. Cyclic voltammogram of the ASSLIBs tested at different scan rates from 0.1 to 0.5 mV s<sup>-1</sup>. Figure S5. Charge and discharge curves of the ASSLIBs assembled (a) without the EI and (b) with 8% of the EI. Cyclability of the ASSLIBs (c) without the EI and (d) with 8% of the EI.

**Author Contributions:** Conceptualization, S.A. and H.-I.K.; formal analysis, M.B.; investigation and resources, M.B. and S.A.; writing—original draft preparation, M.B. and S.A.; writing—review and editing, S.A. and H.-I.K., supervision, H.-I.K., S.Y., J.-k.K., D.K., H.K., and J.P.; project administration, H.-I.K.; funding acquisition, H.-I.K. All authors have read and agreed to the published version of the manuscript.

**Funding:** This work was partly supported by Korea Institute of Energy Technology Evaluation and Planning (KETEP) grant funded by the Korea government (MOTIE) (No. 20224000000070, Human Resource Training For Smart Energy New Industry Cluster). This research was supported by “Regional Innovation Strategy (RIS)” through the National Research Foundation of Korea (NRF) funded by the Ministry of Education (MOE) (2021RIS-001). This research was supported by the Cheongju University Research Scholarship Grants in 2023~2024.

**Institutional Review Board Statement:** Not applicable.

**Informed Consent Statement:** Not applicable.

**Data Availability Statement:** Data is contained within the article.

**Conflicts of Interest:** The authors declare no conflicts of interest.

## References

1. Kim, T.; Song, W.; Son, D.-Y.; Ono, L.K.; Qi, Y. Lithium-ion batteries: Outlook on present, future, and hybridized technologies. *J. Mater. Chem. A* **2019**, *7*, 2942–2964. [[CrossRef](#)]
2. Sanguesa, J.A.; Torres-Sanz, V.; Garrido, P.; Martinez, F.J.; Marquez-Barja, J.M. A Review on Electric Vehicles: Technologies and Challenges. *Smart Cities* **2021**, *4*, 372–404. [[CrossRef](#)]
3. Blomgren, G.E. The development and future of lithium ion batteries. *J. Electrochem. Soc.* **2016**, *164*, A5019. [[CrossRef](#)]
4. Hesse, H.C.; Schimpe, M.; Kucevic, D.; Jossen, A. Lithium-Ion Battery Storage for the Grid—A Review of Stationary Battery Storage System Design Tailored for Applications in Modern Power Grids. *Energies* **2017**, *10*, 2107. [[CrossRef](#)]
5. Manthiram, A. An outlook on lithium ion battery technology. *ACS Cent. Sci.* **2017**, *3*, 1063–1069. [[CrossRef](#)] [[PubMed](#)]
6. Un-Noor, F.; Padmanaban, S.; Mihet-Popa, L.; Mollah, M.N.; Hossain, E. A Comprehensive Study of Key Electric Vehicle (EV) Components, Technologies, Challenges, Impacts, and Future Direction of Development. *Energies* **2017**, *10*, 1217. [[CrossRef](#)]
7. Xu, W.; Zhou, K.; Wang, H.; Lu, L.; Gao, B.; Wang, Y.; Li, Y. Experimental and Modeling Study of Arc Fault Induced Thermal Runaway in Prismatic Lithium-Ion Batteries. *Batteries* **2024**, *10*, 269. [[CrossRef](#)]
8. Chen, Y.; Kang, Y.; Zhao, Y.; Wang, L.; Liu, J.; Li, Y.; Liang, Z.; He, X.; Li, X.; Tavajohi, N.; et al. A review of lithium-ion battery safety concerns: The issues, strategies, and testing standards. *J. Energy Chem.* **2021**, *59*, 83–99. [[CrossRef](#)]
9. Rahmani, A.; Dibaj, M.; Akrami, M. Recent Advancements in Battery Thermal Management Systems for Enhanced Performance of Li-Ion Batteries: A Comprehensive Review. *Batteries* **2024**, *10*, 265. [[CrossRef](#)]
10. Liu, K.; Liu, Y.; Lin, D.; Pei, A.; Cui, Y. Materials for lithium-ion battery safety. *Sci. Adv.* **2018**, *4*, eaas9820. [[CrossRef](#)]
11. Chombo, P.V.; Laonual, Y. A review of safety strategies of a Li-ion battery. *J. Power Sources* **2020**, *478*, 228649. [[CrossRef](#)]
12. Cheng, X.-B.; Zhao, C.-Z.; Yao, Y.-X.; Liu, H.; Zhang, Q. Recent advances in energy chemistry between solid-state electrolyte and safe lithium-metal anodes. *Chem* **2019**, *5*, 74–96. [[CrossRef](#)]
13. Famprikis, T.; Canepa, P.; Dawson, J.A.; Islam, M.S.; Masquelier, C. Fundamentals of inorganic solid-state electrolytes for batteries. *Nat. Mater.* **2019**, *18*, 1278–1291. [[CrossRef](#)]
14. Manthiram, A.; Yu, X.; Wang, S. Lithium battery chemistries enabled by solid-state electrolytes. *Nat. Rev. Mater.* **2017**, *2*, 16103. [[CrossRef](#)]
15. Zhao, Q.; Stalin, S.; Zhao, C.-Z.; Archer, L.A. Designing solid-state electrolytes for safe, energy-dense batteries. *Nat. Rev. Mater.* **2020**, *5*, 229–252. [[CrossRef](#)]
16. Zhang, H.; Liu, X.; Li, H.; Hasa, I.; Passerini, S. Challenges and strategies for high-energy aqueous electrolyte rechargeable batteries. *Angew. Chem. Int. Ed.* **2021**, *60*, 598–616. [[CrossRef](#)] [[PubMed](#)]
17. Jarvis, N.L.; Scheiman, M.A. Surface potentials of aqueous electrolyte solutions. *J. Phys. Chem.* **1968**, *72*, 74–78. [[CrossRef](#)]
18. Wu, F.; Wu, B.; Mu, Y.; Zhou, B.; Zhang, G.; Zeng, L. Metal-Organic Framework-Based Materials in Aqueous Zinc-Ion Batteries. *Int. J. Mol. Sci.* **2023**, *24*, 6041. [[CrossRef](#)]

19. Wang, B.; Xu, H.; Hao, J.; Du, J.; Wu, C.; Ma, Z.; Qin, W. Mini-Review on the Regulation of Electrolyte Solvation Structure for Aqueous Zinc Ion Batteries. *Batteries* **2023**, *9*, 73. [[CrossRef](#)]
20. Reis, S.; Grosso, R.; Kosctiuk, J.; Franchetti, M.; Oliveira, F.; Souza, A.; Gonin, C.; Freitas, H.; Monteiro, R.; Parreira, L.; et al. Effect of Zr<sup>4+</sup> on Lithium-Ion Conductivity of Garnet-Type Li<sub>5+x</sub>La<sub>3</sub>(Nb<sub>2-x</sub>Zrx)O<sub>12</sub> Solid Electrolytes. *Batteries* **2023**, *9*, 137. [[CrossRef](#)]
21. Janek, J.; Zeier, W.G. A solid future for battery development. *Nat. Energy* **2016**, *1*, 16141. [[CrossRef](#)]
22. Janek, J.; Zeier, W.G. Challenges in speeding up solid-state battery development. *Nat. Energy* **2023**, *8*, 230–240. [[CrossRef](#)]
23. Sung, J.; Heo, J.; Kim, D.-H.; Jo, S.; Ha, Y.-C.; Kim, D.; Ahn, S.; Park, J.-W. Recent advances in all-solid-state batteries for commercialization. *Mater. Chem. Front.* **2024**, *8*, 1861–1887. [[CrossRef](#)]
24. Li, C.; Wang, Z.-Y.; He, Z.-J.; Li, Y.-J.; Mao, J.; Dai, K.-H.; Yan, C.; Zheng, J.-C. An advance review of solid-state battery: Challenges, progress and prospects. *Sustain. Mater. Technol.* **2021**, *29*, e00297. [[CrossRef](#)]
25. Zhang, S.; Xu, K.; Jow, T. EIS study on the formation of solid electrolyte interface in Li-ion battery. *Electrochim. Acta* **2006**, *51*, 1636–1640. [[CrossRef](#)]
26. Yu, S.; Schmidt, R.D.; Garcia-Mendez, R.; Herbert, E.; Dudney, N.J.; Wolfenstine, J.B.; Sakamoto, J.; Siegel, D.J. Elastic properties of the solid electrolyte Li<sub>7</sub>La<sub>3</sub>Zr<sub>2</sub>O<sub>12</sub> (LLZO). *Chem. Mater.* **2016**, *28*, 197–206. [[CrossRef](#)]
27. Yu, S.; Siegel, D.J. Grain boundary contributions to Li-ion transport in the solid electrolyte Li<sub>7</sub>La<sub>3</sub>Zr<sub>2</sub>O<sub>12</sub> (LLZO). *Chem. Mater.* **2017**, *29*, 9639–9647. [[CrossRef](#)]
28. Liang, C.C. Conduction characteristics of the lithium iodide-aluminum oxide solid electrolytes. *J. Electrochem. Soc.* **1973**, *120*, 1289–1292. [[CrossRef](#)]
29. Lau, J.; DeBlock, R.H.; Butts, D.M.; Ashby, D.S.; Choi, C.S.; Dunn, B.S. Sulfide solid electrolytes for lithium battery applications. *Adv. Energy Mater.* **2018**, *8*, 1800933. [[CrossRef](#)]
30. Sakuda, A.; Hayashi, A.; Tatsumisago, M. Sulfide solid electrolyte with favorable mechanical property for all-solid-state lithium battery. *Sci. Rep.* **2013**, *3*, 2261. [[CrossRef](#)]
31. Wu, F.; Fitzhugh, W.; Ye, L.; Ning, J.; Li, X. Advanced sulfide solid electrolyte by core-shell structural design. *Nat. Commun.* **2018**, *9*, 4037. [[CrossRef](#)]
32. Fan, X.; Zhong, C.; Liu, J.; Ding, J.; Deng, Y.; Han, X.; Zhang, L.; Hu, W.; Wilkinson, D.P.; Zhang, J. Opportunities of flexible and portable electrochemical devices for energy storage: Expanding the spotlight onto semi-solid/solid electrolytes. *Chem. Rev.* **2022**, *122*, 17155–17239. [[CrossRef](#)] [[PubMed](#)]
33. Lu, X.; Wang, Y.; Xu, X.; Yan, B.; Wu, T.; Lu, L. Polymer-Based Solid-State Electrolytes for High-Energy-Density Lithium-Ion Batteries—Review. *Adv. Energy Mater.* **2023**, *13*, 2301746. [[CrossRef](#)]
34. An, Y.; Han, X.; Liu, Y.; Azhar, A.; Na, J.; Nanjundan, A.K.; Wang, S.; Yu, J.; Yamauchi, Y. Progress in solid polymer electrolytes for lithium-ion batteries and beyond. *Small* **2022**, *18*, 2103617. [[CrossRef](#)]
35. Wu, Y.; Li, Y.; Wang, Y.; Liu, Q.; Chen, Q.; Chen, M. Advances and prospects of PVDF based polymer electrolytes. *J. Energy Chem.* **2022**, *64*, 62–84. [[CrossRef](#)]
36. Alipoori, S.; Mazinani, S.; Aboutalebi, S.H.; Sharif, F. Review of PVA-based gel polymer electrolytes in flexible solid-state supercapacitors: Opportunities and challenges. *J. Energy Storage* **2020**, *27*, 101072. [[CrossRef](#)]
37. Vijayakumar, V.; Anothumakkool, B.; Kurungot, S.; Winter, M.; Nair, J.R. In situ polymerization process: An essential design tool for lithium polymer batteries. *Energy Environ. Sci.* **2021**, *14*, 2708–2788. [[CrossRef](#)]
38. Laouchedi, D.; Bezzazi, B.; Aribi, C. Elaboration and characterization of composite material based on epoxy resin and clay fillers. *J. Appl. Res. Technol.* **2017**, *15*, 190–204. [[CrossRef](#)]
39. Hashemifard, S.; Ismail, A.; Matsuura, T. Effects of montmorillonite nano-clay fillers on PEI mixed matrix membrane for CO<sub>2</sub> removal. *Chem. Eng. J.* **2011**, *170*, 316–325. [[CrossRef](#)]
40. Dong, H.; Wu, L.; Zhang, L.; Chen, H.; Gao, C. Clay nanosheets as charged filler materials for high-performance and fouling-resistant thin film nanocomposite membranes. *J. Membr. Sci.* **2015**, *494*, 92–103. [[CrossRef](#)]
41. Pluta, M.; Paul, M.A.; Alexandre, M.; Dubois, P. Plasticized polylactide/clay nanocomposites. I. The role of filler content and its surface organo-modification on the physico-chemical properties. *J. Polym. Sci. Part B Polym. Phys.* **2006**, *44*, 299–311. [[CrossRef](#)]
42. Ray, S.; Easteal, A.J. Advances in Polymer-Filler Composites: Macro to Nano. *Mater. Manuf. Process.* **2007**, *22*, 741–749. [[CrossRef](#)]
43. Zhen, R.; Chi, Q.; Wang, X.; Yang, K.; Jiang, Y.; Li, F.; Xue, B. Crystallinity, ion conductivity, and thermal and mechanical properties of poly(ethylene oxide)-illite nanocomposites with exfoliated illite as a filler. *J. Appl. Polym. Sci.* **2016**, *13*, 44226. [[CrossRef](#)]
44. Zhen, R.; Jiang, Y.S.; Li, F.F.; Xue, B. A study on the intercalation and exfoliation of illite. *Res. Chem. Intermed.* **2017**, *43*, 679–692. [[CrossRef](#)]
45. Ashurov, M.S.; Bakhia, T.; Saidzhonov, B.M.; Klimonsky, S.O. Preparation of inverse photonic crystals by ETPTA photopolymerization method and their optical properties. *J. Phys. Conf. Ser.* **2020**, *1461*, 012009. [[CrossRef](#)]

**Disclaimer/Publisher's Note:** The statements, opinions and data contained in all publications are solely those of the individual author(s) and contributor(s) and not of MDPI and/or the editor(s). MDPI and/or the editor(s) disclaim responsibility for any injury to people or property resulting from any ideas, methods, instructions or products referred to in the content.